

# Microwave Emissivity over Ocean in All-Weather Conditions. Validation Using WINDSAT and Airborne GPS-Dropsondes

Sid-Ahmed Boukabara, *Senior Member, IEEE*, and Fuzhong Weng

**Abstract**—Emissivity spectra computed by the FASTEM-3 model using GPS-dropsonde wind as input, are compared to emissivity retrieved from stringently coincident WINDSAT measurements, using a variational approach. This is done in both clear and rainy conditions to assess the validity of both the emissivity model and the retrieval technique in all conditions. Results of this comparison are presented for vertical and horizontal polarizations, in moderate to high winds conditions. In particular, a slope difference is found and its potential sources discussed in this study.

**Index Terms**— Microwave emissivity, Retrieval algorithm, Variational assimilation, Dropsonde, Hurricane.

## I. INTRODUCTION

The microwave emissivity modeling over sea surfaces has experienced significant advances in the last decades and is now considered a well handled issue [English, 2006]. Most operational centers use a microwave emissivity model in the assimilation process of surface-sensitive channels, for the purpose of producing sea surface wind intensities and/or directions [Ruston and Boukabara, 2006]. A large number of emissivity models have been published in the literature, some based on empirical expressions but fast and some with explicit treatment of the surface geometry but with a high computation cost that prevents them from being used operationally [Stogryn 1967, Wilheit 1979, Wentz 1983, Prigent and Abba 1990, Guissard et al. 1992, English and Hewison 1998, Boukabara 2002]. There are however remaining issues in the emissivity modeling related to uncertainties in the dielectric constant modeling, the foam emissivity and coverage parameterizations and the nature of the relationship between the wind and the surface geometry [Camps et al, 2005, Azziz et al. 2005,

Padmanabhan et al. 2006]. There are also wide open uncertainties on the accuracy of the emissivity models in rainy conditions [Bliven et al. 1997, Camps et al. 2001, Craeye et al. 2003]. In these conditions, the sea roughness is altered by the amount of rain and the size distribution of the precipitation. In addition, the atmospheric signal is impacted by attenuation and scattering of the rain which also freshens the surface.

On the other hand, direct retrievals of emissivity spectra from brightness temperatures have been performed, particularly over land but also over ocean, using variational approaches or analytical methods [Moncet et al. 1995, Karbou et al. 2005]. In this study, we undertook to compare retrievals of emissivity spectra from WINDSAT data ranging from 6 to 37 GHz, to emissivity model simulations using airborne GPS-dropsonde measurements of wind intensity. These latter were provided to us by the Hurricane Research Division in Miami, FL. They are taken routinely during Hurricane events, in and around the active area where airplanes are flown to probe the storm intensity and other parameters. They provide temperature, humidity and wind vertical profiles, down to a few meters from the surface level. The variational algorithm used to retrieve the emissivity is called the Microwave Integrated Retrieval System (MIRS) [Boukabara et al. 2006] where the emissivity spectrum is part of the retrieved state vector. The use of the Community Radiative Transfer Model (CRTM) as the forward operator in MIRS makes it possible to perform the retrieval in all-weather conditions including precipitating ones. Both radiances and Jacobians are provided by CRTM. The problem is ill-constrained but this is alleviated by performing the retrieval in a reduced space, selecting only a limited number of degrees of freedom (Eigenvalues).

## II. MICROWAVE EMISSIVITY MODEL

The microwave emissivity modeling of the sea surface depends on a number of parameters: the dielectric constant for saline water, the surface geometry or roughness and the foam emissivity and coverage. The dielectric constant is itself dependent on the water temperature and the salinity. The effect of this latter for high frequency channels is known to be negligible [Guillou et al. 1998, Meissner and Wentz 2004]. The surface roughness is usually modeled by parameterizing the surface large and/or small wave slopes distribution which is mostly dependent on the surface wind vector. The

Manuscript received February 15, 2007, revised XXX 2007, accepted YYY 2007. The views expressed in this publication are those of the authors and do not necessarily represent those of the National Oceanic and Atmospheric Administration (NOAA).

S-A. Boukabara is with NOAA/NESDIS/STAR, Camp Springs, MD 20746 USA (e-mail: Sid.Boukabara@noaa.gov).

F. Weng is with the NOAA/NESDIS/STAR, Camp Springs, MD 20746 USA (e-mail: Fuzhong.Weng@noaa.gov).

relationship between the wind and the wave distribution usually assumes neutral stability. The Geometric Optics (GO) models assume that the emissivity is mainly dependent on the large length waves (larger than the sensor wavelength) and ignore the small scale variability. Two-scale models do account for these small perturbations by using the small perturbation method (SPM) but are time-prohibitive. The foam is not very well modeled and usually depends on regression fits to wind speed. It is neglected in most models for low wind speeds and large uncertainties exist for high wind regimes [Camps et al. 2005, Padmanabhan et al. 2006]. The emissivity model used in this study is the newest version of the FASTEM model. This latter is a fast GO model that was originally called FASTEM-1 [English and Hewison, 1998] and was designed to compute ocean surface emissivity given a sea surface temperature, wind speed and viewing angle for a microwave radiometer channel. Deblonde and English (2001) then developed an improved version called FASTEM-2 which takes into account the treatment of non-specular reflection. This had the effect of improving the simulation of ocean surface emissivity for SSM/I and AMSU for larger viewing angles as described in Deblonde (2000). FASTEM-2 has been further updated to allow for the dependence of the ocean surface emissivity on the azimuth angle between the wind direction and the line of sight of the instrument. The resulting FASTEM-3 is also able to predict the behavior of the 3<sup>rd</sup> and 4<sup>th</sup> elements of the Stokes vector as a function of wind speed and wind direction. The azimuthal variation of emissivity was based on an empirical model [Liu and Weng, 2003]. The surface wave distribution in FASTEM-3 is based on a fast regression fit.

### III. RETRIEVAL/ASSIMILATION SYSTEM

The inversion system used in this study is a generic variational retrieval algorithm (1DVAR) that applies to all microwave sensors with no change to the code. The retrieval of the temperature and moisture profiles is done along with the precipitating and non-precipitating cloud parameters. The surface boundary is handled by including the surface emissivity and temperature within the retrieval state vector. To alleviate the limited information content available in the instrument at hand, the inversion is performed in a reduced Eigenvalue space as mentioned before, which makes the retrieval process stable and mathematically consistent. The mathematical basis of MIRS is a proven and widely used variational approach described in (Rodgers 1976), consisting of minimizing the following cost function (1):

$$J(X) = \left[ \frac{1}{2} (X - X_0)^T \times B^{-1} \times (X - X_0) \right] + \left[ \frac{1}{2} (Y^m - Y(X))^T \times E^{-1} \times (Y^m - Y(X)) \right]$$

The first right term  $J_b$  represents the penalty in departing from the background value (a-priori information) and the second right term  $J_r$  represents the penalty in departing from the measurements.  $X_0$  and  $B$  are the mean vector (or background) and covariance matrix of the state vector  $X$ , respectively.  $E$  is the measurement and/or modeling error covariance matrix. The measurements vector is represented by  $Y^m$  and  $Y$  is the forward operator. The following is the solution to the cost function

minimization process, where  $n$  is the iteration index (a maximum number of seven iterations is allowed).

$$\Delta X_{n+1} = \{BK_n^T (K_n BK_n^T + E)^{-1}\} [(Y^m - Y(X_n)) + K_n \Delta X_n] \quad (2)$$

$K$  in this case is the Jacobian or derivative of  $Y$  with respect to  $X$ . At each iteration  $n$ , the new optimal departure from the background is computed, given the derivatives as well as the covariance matrices. This is an iterative-based numerical solution that accommodates moderately non-linear problems or/and parameters with moderately non-Gaussian distributions. The whole geophysical vector is retrieved as one entity including the temperature, moisture and hydrometeors parameters as well as skin surface temperature and emissivity vector, ensuring a consistent solution that fits the radiances. In the case of non-sounder sensors, like WINDSAT, the temperature and humidity profiles are still part of the retrieved vector but they are usually not varied and remain close to the background values. In practical terms, only 1 or 2 Empirically Orthogonal Functions (EOFs) are used for the vertical profiles and the net effect is that the water vapor profile is simply scaled so that only the integrated water vapor gets changed. The forward operator CRTM used in MIRS was developed at the Joint Center for Satellite Data Assimilation (JCSDA) [Weng et al. 2005] and produces radiances as well as Jacobians, for all geophysical parameters. Derivatives are computed using K-matrix developed by Tangent Linear (TL) and Adjoint (AD). This is ideal for retrieval and assimilation purposes. The different components of CRTM briefly are the OPTRAN fast atmospheric absorption model (McMillin et al. 1995), and the advanced doubling adding radiative transfer solution for the multiple-scattering modeling (Liu and Weng 2006). The convergence criterion used in MIRS is:

$$\varphi^2 = \left[ (Y^m - Y(X))^T \times E^{-1} \times (Y^m - Y(X)) \right] \leq N \quad (3)$$

Where  $N$  is the number of channels used for the retrieval process. This mathematically means that the convergence is declared reached if the residuals between the measurements and the simulations at any given iteration are less or equal than one standard deviation of the noise that is assumed in the radiances.

### IV. INSTRUMENTAL CONFIGURATION

In this study we will use the wind-dedicated mission WINDSAT onboard to CORIOLIS platform, which was launched on January 2003, as it offers the opportunity to assess the emissivity modeling in frequencies from 6.8 to 37 GHz in both horizontal and vertical polarizations. The WINDSAT sensor measures primarily the ocean surface wind field at a horizontal resolution of 25 km. The secondary measurements of WINDSAT are the sea surface temperature, the soil moisture, the rain rate, the integrated cloud, the ice/snow characteristics and the water vapor. The WINDSAT radiometer has five channels at 6.8, 10.7, 18.7, 23.8, and 37.0 GHz. Table 1 provides key characteristics of the system. The antenna beams view the Earth at incidence angles ranging from 50 to 55°. The orbit and antenna geometry result in a forward-looking swath of approximately 1000 km and an aft-looking

swath of about 350 km. Data used in this study were processed at Fleet Numerical Meteorology and Oceanography Center (FNMOC) and made available through the Jet Propulsion Laboratory (JPL).

Band (GHz)	Polarization	Bandwidth (MHz)	Earth Incidence Angle (deg)	Horizontal Spatial Resolution(km)
6.8	V,H	125	53.5	40x60
10.7	V,H, $\pm$ 45, L,R	300	49.9	25x38
18.7	V,H, $\pm$ 45, L,R	750	55.3	16x27
23.8	V,H	500	53.0	12x20
37.0	V,H, $\pm$ 45, L,R	2000	53.0	8x13

Table 1. WINDSAT Characteristics (source: NRL/Navy)

## V. INFORMATION CONTENT ASSESSMENT

Sensitivities of WINDSAT measurements to emissivity in all-weather condition was assessed and is presented here. It is important to assess this information content because variational algorithms could retrieve products only because of correlations with other derived products and not really because of the existence of a radiance signal. These correlations are contained within the covariance matrix  $B$ . To determine if we really do have signal in our measurements, under precipitating conditions, we computed the Jacobians (using CRTM) of brightness temperature with respect to emissivity for varying atmospheric water vapor (TPW) values, for a range of rain water path and for a number of cloud amount/ice amount combinations. The total precipitable water (TPW) was varied between 2 and 80 mm, the vertically integrated rain water path (RWP) was varied between 0 and 0.6 mm, for cloud amounts of 0 (clear sky) and 1 mm and for graupel-size ice vertical amounts of 0 and 0.6 mm. This is presented in Figure 1 for the 37 GHz channel. Typically, lower frequency channels present higher signal (not shown). The results show that clear sky situations (no cloud, no rain, no ice) present the highest sensitivity as one might expect. The ice effect is minimal in this channel, also as expected. This frequency is indeed not very sensitive to scattering by ice. The absorption effect due to cloud and rain is to significantly reduce the sensitivity to surface. This reduction is modulated by the amount of humidity in the atmosphere. The lowest sensitivity, approximately 0.4 Kelvin for a 0.01 emissivity change, is found for the most humid and most intense precipitation cases. The strongest sensitivity in clear sky cases reaches 1.5 Kelvin per 0.01 emissivity change. The main conclusion of this analysis is that reasonable signal remains in the WINDSAT channels even when heavy precipitation is present, making it possible to retrieve emissivity in these conditions.

A similar sensitivity study was performed for all AMSU and MHS channels (not shown) that indicate that saturation occur very rapidly in channels with frequencies at 89 GHz and higher, making the retrieval of higher frequency emissivities in a variational algorithm, totally dependent on the built-in

correlations between the low-frequency and high-frequency emissivities. It is therefore difficult to assess emissivity model validity at high frequencies in rainy / cloudy conditions.

## VI. CASE STUDY

In order to test with real data and attempt validation, we need a source of ground truth data which simultaneously provides atmospheric temperature, water vapor and of course wind speed. The vertical profiles are used to side-assess other parameters such as TPW which are by-products of the variational algorithm but not the focus of this study. This constitutes an additional piece of information in the validation of the emissivity. The standard buoy measurements offer the wind information but lack the atmospheric component. The standard radiosondes on the other hand offer the measurements of atmospheric profiles but no information of the wind. High quality airborne dropsondes, such as those provided by the Hurricane Center in Florida, offer a unique opportunity by providing simultaneous measurements of temperature, moisture and wind profiles. In fast moving conditions such as in precipitating cells, the time and space collocation errors could be very significant and may overshadow any validation assessment we might attempt. Therefore very stringent collocation criteria must be used. We focused our study on the 2005 Hurricane Dennis which devastated Cuba and Haiti before making land fall in the US Gulf coast on July 10<sup>th</sup>. The general view of that hurricane is presented in Figure 2 and Figure 3 from the WINDSAT measurements and from a single channel of the MHS sensor (157 GHz). The WINDSAT signatures are presented for all H polarization from 6.8 GHz to 37 GHz. On top of the brightness temperature fields are overlaid a number of airborne dropsondes launch spots. The horizontal color bar represents the brightness temperature intensity while the vertical bar represents the time difference between these dropsondes and the satellite measurements. It is obvious that the atmospheric effect on the WINDSAT measurements is to increase the signal due to cloud and rain absorption (no ice scattering). This increase is proportional to the frequency. The MHS channel at 157 on the other hand experiences a significant scattering effect due to hydrometeors (Figure 3). The signal tends to drop in the middle of the rainy cell for this channel.

## VII. VALIDATION USING GPS-DROPSONDES

Coriolis/WINDSAT sensor was used to compare retrievals of emissivity generated using the variational algorithm described above with airborne-based GPS-dropwindsondes, in both clear cases as well as under precipitating conditions. It is critical that one gets a clear sense of how accurate the *truth* measurements (in our case, dropsondes) are before interpreting any differences between them and the retrievals.

### A. GPS-DropWindSondes

These measurements are made in cloudy/rainy conditions (typically during hurricanes and tropical storms) by high velocity descending GPS-dropsondes. These latter were quality-controlled using the Hurricane Analysis and Processing System (HAPS) [Hock and Franklin 1999]. They operate at

altitudes up to 24 kms with a descent time of about twelve minutes. The measurements are made every half second which allows a high vertical resolution. Along with the temperature and moisture, the vertical wind speed profile is also measured by using GPS-based Doppler signal, down to 4-10 meters above the surface. The validation of these dropsondes was assessed by comparison with standard radiosondes, radars, buoys as well as by human visualization of clouds for the saturation check. For a full description of these measurements, see [Hock and Franklin 1999]. For the wind, an accuracy of 0.5-2 m/s was estimated. Figure 4 shows the locations of the dropsondes when they were dropped from the airplane during hurricane Dennis. It also highlights the individual sondes selected for a case-by-case comparison in the next section. It was reported by [Hock and Franklin 1999] that almost-coincident measurements of wind profiles by successive dropsondes were made to assess the precision of the wind from these sondes. The main conclusion was that the coincident sondes always reported differences less than 1 m/s but they mention that in cases of poor GPS geometry accuracy, the differences may reach 2 m/s.

### B. Limitations of the validation in extreme weather events

Traditional approach to validating retrievals or models by statistical comparison with ground truth data collected around the measurement's time/space location is not optimal in the case of hurricane conditions. The main reason is the fast moving features involved. Collocation errors are expected to be dominant in very active areas. Stringent time and space criteria must therefore be used, which obviously dramatically reduces the total number of coincident collocations. This in turn renders the empirical assessment statistically meaningless at best or practically unfeasible at worst. Note that the tight time and space collocation must be between coincident satellite measurements, hurricane events and ground truth such as dropsondes.

One of the challenges faced during this comparison is the fact that emissivity models usually require 10-meters height wind and assume local thermodynamical stability, which is not necessarily valid under precipitating conditions. The GPS-based wind profile sometimes goes down to 10 meters but sometimes does not for various reasons. The approach adopted in this study was to select the reported wind closest to 10 meters height. The difference in height will contribute to the uncertainty errors. Another type of limitation one should be aware of is what other studies called representativeness error which relates to the fact that dropsonde measurements are point-measurement and do not necessarily represent what the sensor is measuring within the whole field of view of the spaceborne sensor. Unfortunately, the number of dropsondes collocated with satellite measurements is limited and therefore the luxury of averaging within the footprint to mitigate representativeness errors (or around the time of the measurement) can not be afforded.

### C. Case-By-Case Validation

Given the limitations discussed above, and for the purpose of the model versus retrieval comparison, it was critical to find

the *as-perfect-as-possible* collocation between the satellite measurements and the GPS-dropsondes. Figure 5 shows a field of the convergence metric ( $\varphi^2$ ) using two retrievals, one with the multiple scattering capability turned ON and one with the capability turned OFF. The retrieval was done using all WINDSAT channels simultaneously. This shows how important it is to account for precipitation effects when performing retrievals in rainy conditions, even when frequencies involved are all low (below 37 GHz). Non-precipitating cloud is not able, alone, to compensate for precipitation. Notice that very heavy rain (at rain bands) still exhibits non-convergence which suggests that either (1) the forward model is not accurate enough in these regions or that (2) the assumed instrument errors are not representative (too low) or even that (3) the hydrometeors covariance is not applicable or close enough to the particular case studied here. Note also that non-convergence extends to coastal areas. This is to be expected because the emissivity covariance matrix does not represent at all these cases. Figure 6 and Figure 7 present the comparison between several emissivity spectra in clear and precipitating conditions respectively. These individual dropsonde cases were selected in Figure 4. In both cases, the retrieval reached convergence, i.e. the resulting emissivities (along with the rest of the state vector) fit the measurements within noise levels.

The spectra displayed in these figures are (1) two retrieved spectra from the MIRS system using non-corrected WINDSAT brightness temperatures and in which the scattering model was turned ON or OFF, (2) the computed emissivity spectrum using the FASTEM-3 model and the dropsonde wind as input (the wind closest to 10-meters height), (3) the emissivity spectrum simulated using FASTEM-3 and GDAS analysis wind as input (included for reference). (4) The background emissivity spectrum is also plotted for reference to highlight what type of spectral constraint we had during the retrieval. The background emissivity constraints over ocean are built using the same FASTEM-3 model, which is part of the CRTM package we use in the retrieval algorithm.

## VIII. RESULTS

In Figure 6 (clear sky case), the individual dropsonde measured the wind at a height of 8 meters. The MIRS retrieved surface temperature (301.5K) is roughly similar to the one from the GDAS analysis field (302 K). The distance difference between the dropsonde (DS) and the satellite measurement footprint center was 4.4 Km. The time difference was 1.7 hours. The GDAS reported wind was 6.7 m/s while the dropsonde reported 8.4 m/s. The closeness of surface temperature and wind reportings between the DS and the GDAS is to be expected as GDAS does assimilate those dropsonde measurements. This in turn explains why the corresponding simulated emissivity spectra are close. The two MIRS-based retrieved spectra (using absorption only and accounting for the full extinction effects) are undistinguishable, confirming that no heavy precipitation was taking place for this individual case. In other words, turning ON or OFF the precipitation handling does not make a difference in the retrieved emissivity. It is worth noting that the

retrieved spectrum is departing from the background spectrum in both V and H, consistently, responding therefore to signal from the brightness temperature measurements. The retrieved spectrum adopted a slightly larger spectral slope than both the background and the FASTEM-3 based emissivity (with the GPS-dropsonde wind as input). For V polarization, the low frequency (between 6 and 19 GHz) emissivity values are relatively similar between the retrieved spectrum and the DS&FASTEM3-based values. The departure between the spectra reaches a maximum at 37 GHz with the retrieved emissivity being higher by as much as 0.04 than the DS&FASTEM value. For the H polarization, the slight slope difference (same direction) is creating differences in the low and high ends of the frequency range but they do not exceed 0.02. It is important to recall that the retrieval has reached convergence in this case and is therefore producing final brightness temperatures consistent with the measurements. The individual channels residuals were around 2 K for the V channels and 0.8 K for the H channels, with an overall  $\phi^2$  of 1.

Figure 7 represents another case of comparison, corresponding to precipitating conditions previously identified in Figure 4. It is worth noting that in this case, the retrieved spectra with and without accounting for the full extinction due to precipitation, are clearly distinct, which confirms that the case is indeed affected by rain. In this case, the reported skin temperature by GDAS was 301.8 K and that retrieved by MIRS was 303.4 K, a difference of 1.6 K. The wind reported by GDAS was 7.9 m/s while the one reported by the dropsonde was much higher at 12.1 m/s. It is expected that assimilation-based wind is underestimated in the high end as this is a smoothed value within a grid, while the dropsonde measurement is a point-measurement that has much more spatial variability. The collocation for this case was almost perfect: less than 15 minutes in time and less than 6 km in distance, reducing the collocation errors to a minimum. However, the DS wind was reported at 16 m. It is interesting to note that similar features found in the clear case, are reproduced in this case as well. In particular, the retrieved spectrum (we focus on the scattering-ON one) tends to have a higher spectral slope (than the model) in both V and H channels, but with more dramatic differences than in the case of clear conditions. It is found that low frequency emissivity values in the V case tend to be similar between the FASTEM-3 simulations and the retrieved values, but tend to depart more quickly and reach a maximum difference of 0.05 at 37 GHz. In the case of the H-polarization channels, the same remark found in the clear conditions could also be drawn, i.e. that the slight difference in the spectral slope introduces differences in the low and high end of the [6-37GHz] frequency range but with differences less than 0.02. It is similarly important to note that the retrieval had reached convergence in this case as well, with residuals (not shown) being around 3 K for the case of V-pol channels and around 1.5 K in the case of H-pol channels.

## IX. DISCUSSIONS

The comparisons between FASTEM3-based emissivity spectra and MIRS-retrieved ones, presented here, are consistent with other individual cases not shown. They reveal a spectral slope

anomaly: the retrieved emissivity spectrum shows a higher slope than that of the model. By focusing on individual cases, we have reduced the time and space collocation errors to a strict minimum. This was done in order to isolate only the retrieval and emissivity model errors.

The first potential source of discrepancy that comes to mind is the difference between the wind speed measured by the DS and the composite wind speed the sensor views within the field of view. But this difference would have generated a bias across the spectrum and not such a distinct slope. This could be confirmed by the emissivity spectra computed using the different winds, the one from DS and the one from GDAS (see Figure 7). This wind input difference is similar in nature to the difference due to the reporting at a height different from expected 10-meters. By the same token, skin temperature difference, besides being small, could not generate such a slope anomaly. An alternative explanation might be that the foam coverage and emissivity are larger in nature than those predicted by the emissivity model. Foam is known to have much higher emissivity (close to a black body) than saline water. In their study, [Rose et al. 2002] found that while at 10 GHz, model foam emissivity were close to their measurements, at 36.5 GHz, there was a significant underestimation of the model. Another source of potential source for this difference in slope is the uncertainty associated with the sea-water dielectric constant model. There is indeed a discrepancy in the literature about the dielectric constant. At high frequencies (85 GHz), there seems to be consensus that work by [Guillou et al. 1998] extended later by [Lamkaouchi et al. 2003, Ellison et al. 2003], based on laboratory measurements, provides better results than that of [Klein and Swift 1977], but at low frequencies, discrepancies are reported by [Meissner and Wentz, 2004] based on SSM/I data. In their study, differences between measurements and simulations at 19, 22 and 37 GHz channels showed that differences between [Guillou et al. 1998] model (similar to that employed in FASTEM) and SSMI radiances generate differences that increase with frequency (~1.5 K at 19/22 and ~3K around 37 GHz). Little differences were found at 85 GHz. The differences were modulated by the surface temperature. The assumption of atmospheric thermodynamic stability at the air-sea interface is an additional source of uncertainty that could explain this slope anomaly. [Gianpaolo and Ruf 2001] showed that air-sea temperature difference had indeed an impact on the wind emissivity slope and that impact varied significantly with frequency (they used a [18-37 GHz] frequency range). Even if their study was performed at nadir, it might be that these instabilities, not accounted for in the model, are creating frequency-dependent differences and therefore a spectral slope anomaly. There is obviously the uncertainty in the sea surface geometry and its unique link to near-surface wind speed that might also be causing the slope discrepancy. Roughness of the surface is generally due to gravity and capillary waves, which are sensitive to wind and their dissipation depends on viscosity. But other parameters play a role influencing one or both types of waves: fetch, swell, non-stationary wind, sea development stage. The small scale waves of the surface are known to impact low frequencies and therefore their uncertainty might be a cause for the slope anomaly found between the DS-based and MIRS-

based spectra. FASTEM uses a simplified term to account for Bragg scattering following [Choudhury et al. 1979].

The spatial resolution could be another source leading indirectly to that emissivity slope discrepancy: The lower frequencies having larger footprints, the relative impact of the same rainy cell could be different from that on a high-frequency channel with a smaller footprint. This could result in a rain-effect with frequency dependence feature. This reasoning applies however only to isolated rain cells or isolated cloud patches. In case of spatially uniform field distribution of rain and cloud, the relative effect of the footprint should be independent of footprint size and therefore of frequency. This is because the relative cloud/rain fraction within the footprint will be the same.

Another type of potential sources for this discrepancy lies in the variational retrieval. Errors in the cloud amount retrieved could be compensated for by surface emissivity. The optical properties of the scatterers retrieved, if not modeled properly could also be a potential source for generating this emissivity spectra discrepancy. Similarly, if the water vapor continuum is not correct, or more exactly, inconsistent with the measurements, its signature, bound to be frequency dependent, might end up in the retrieved emissivity spectrum. A spectral discrepancy between the measured brightness temperatures (cross-channels mis-calibration) could also be causing this emissivity slope anomaly. It is interesting to notice that both the clear and rainy cases exhibit similar features, suggesting that the general emissivity model may potentially be applicable under those precipitating events provided perhaps a light tuning. Although it is not possible to conclude based on a limited number of cases, it seems that the impact of rain-induced roughness is minimal, judging from the relative behavior of the emissivity model and the retrieved emissivity spectrum.

In general, within the uncertainties identified, on both the emissivity model side and the variational retrieval side, it is found that the emissivity model agrees with the retrieved spectra within 0.02 for H-pol channels in the [6-37 GHz]. For V-pol channels, the differences are also within 0.02 in the more limited range of [6-19 GHz]. Above 19 GHz, the difference increases almost linearly to reach a maximum of 0.04 in clear (0.05 in rainy) case. This was obtained in moderate to relatively high wind conditions.

#### ACKNOWLEDGMENT

Authors gratefully acknowledge S. Feuer and M.L. Black from the Hurricane Research Division (HRD) of the NOAA Atlantic Oceanographic and Meteorological Laboratory (AOML) for kindly providing the dropsondes data. The JCSDA CRTM team (Q. Liu, Y. Han and P. Van Delst) is also acknowledged for providing an early version of the radiative transfer model CRTM.

## REFERENCES

- [1] M.A. Aziz; Reising, S.C.; Asher, W.E.; Rose, L.A.; Gaiser, P.W.; and Horgan, K.A., "Effects of air-sea interaction parameters on ocean surface microwave emission at 10 and 37 GHz", IEEE Transactions on Geoscience and Remote Sensing, Volume 43, Issue 8, Aug. 2005 Page(s):1763 – 1774. DOI 10.1109/TGRS.2005.848413
- [2] S.A. Boukabara, L. Eymard, C. Guillou, D. Lemaire, P. Sobieski and A. Guissard. "Development of a modified two-scale electromagnetic model, simulating both active and passive microwave measurements. Comparison to data remotely sensed over the ocean". Radio Science, Vol. 37, N4, 10.1029/1999RS002240, 2002.
- [3] S-A. Boukabara , F. Weng , R. Ferraro , L. Zhao , Q. Liu , B. Yan , A. Li , W. Chen , N. Sun , H. Meng , T. Kleespies , C. Kongoli , Y. Han , P. Van Delst , J. Zhao and C. Dean. *Introducing NOAA's Microwave Integrated Retrieval System (MIRS)*, 15<sup>th</sup> International TOVS Satellite Conference (ITSC-15), Maratea, Italy, 2006.
- [4] F.L. Bliven, P. Sobieski and C. Craeye, "Rain generated ring-waves: measurements and modeling for remote sensing", International Journal of Remote Sensing, Vol 18, No 1, pp. 221-228, 1997.
- [5] A. Camps, A. Vall-Ilossera, M. Miranda, J. Duffo, N. "Emissivity of the sea surface roughened by rain: simulation results". Geoscience and Remote Sensing Symposium, IGARSS2001. pp: 2433-2435, vol.5, Sydney, Australia, DOI: 10.1109/IGARSS.2001.978026, 2001
- [6] A. Camps; Vall-Ilossera, M.; Villarino, R.; Reul, N.; Chapron, B.; Corbella, I.; Duffo, N.; Torres, F.; Miranda, J.J.; Sabia, R.; Monerris, A. and Rodriguez, R., "The emissivity of foam-covered water surface at L-band: theoretical modeling and experimental results from the FROG 2003 field experiment", IEEE Transactions on Geoscience and Remote Sensing, Volume 43, Issue 5, May 2005 Page(s):925 – 937. DOI 10.1109/TGRS.2004.839651
- [7] B.J. Choudhury, Schumge, T. J., Newton, R. W., and Chang, A. T. C., "Effect of surface roughness on microwave emission of soils". *J. Geophys. Res.*, 84, 5699-5706, 1979
- [8] C. Craeye, C. Sobieski, P. and Bliven, L.F. , "A relationship between atmospheric rain reflectivity and elevation variance due to drop impact on the sea surface", Oceans 2003 proceedings, vol.1, pp 528-531, DOI: 10.1109/OCEANS.2003.178634, 2003
- [9] G. Deblonde and S.J. English "Evaluation of the FASTEM-2 fast microwave oceanic surface emissivity model". *Tech. Proc. ITSC-XI Budapest, 20-26 Sept 2000* 67-78, 2001
- [10] W.J. Ellison, S.J. English, K. Lamkaouchi, A. Balana, E. Obligis, G. Deblonde, T.J. Hewison, P. Bauer, G. Kelly and L. Eymard, "A comparison of ocean emissivity models using the advanced microwave sounding unit, the special sensor microwave imager, the TRMM Microwave imager and airborne radiometer observations", *J. of Geophys. Research*, vol. 108, No D21, 4663, 2003
- [11] S. English and T. J. Hewison "A fast generic millimeter-wave emissivity model". *Microw. Rem. Sens. of the Atm. Environ.*, SPIE, 3503, 22-30, 1998.
- [12] S. English. "Issues in ocean emissivity modelling", Talk at the 1<sup>st</sup> Workshop on Remote Sensing and Modeling of Surface Properties, Paris, France, June, 2006. <http://cimss.ssec.wisc.edu/itwg/groups/rtwg/meetings/sfcem/>
- [13] J. C. Giampaolo and Christopher S. Ruf, "The Effect of Atmospheric Stability on Microwave Excess Emissivity Due to Wind". IEEE Trans. on Geosc. and Remote Sensing, Volume: 39, 10 , pp: 2311- 2314, 2001.
- [14] C. Guillou, W. Ellison, L. Eymard, K. Lamkaouchi, C. Prigent, G. Delbos, G. Balana and S.A. Boukabara., "Impact of new permittivity measurements on sea surface emissivity modeling in microwaves". Radio Science, **33**(3): p. 649 – 667, 1998.

- [15] A. Guissard, Sobieski P. and Baufays C., "A unified approach to bistatic scattering for active and passive remote sensing of rough ocean surfaces", Trends in Geoph.ys. Res., vol.1, pp 43-68, 1992
- [16] T.F. Hock and J. L. Franklin, "The NCAR GPS Dropwindsonde", *Bull. Amer. Meteor. Soc.*, vol. 80, No. 3, 407-420, 1999
- [17] F. Karbou, Prigent, C. Eymard, L. Pardo, J.R. "Microwave land emissivity calculations using AMSU measurements". IEEE Trans. on Geosc. and Remote Sensing, Volume: 43, 5 , pp: 948- 959, 2005.
- [18] L.A. Klein and C.T. Swift, "An improved model for the dielectric constant of sea water at microwave frequencies", IEEE. Trans. Antenna and Propag., 25, 104-111, 1977
- [19] K. Lamkaouchi, A. Balana, G. Delbos and W. Ellison, "Permittivity measurements of lossy liquids in the frequency range 20-110 GHz", Meas. Sci. Technol., 14, 1-7, 2003
- [20] Q. Liu and F. Weng, "Retrieval of sea surface wind vectors from simulated satellite microwave polarimetric measurements", Radio Science, vol. 38, pp. 8078-8085, 2003
- [21] Q. Liu, and F. Weng, "Advanced Doubling-Adding Method for Radiative Transfer in Planetary Atmospheres", J. Atmos. Sci., Accepted, 2006
- [22] L.M. McMillin, L.J. Crone and T.J. Kleespies, "Atmospheric transmittance of an absorbing gas. 5. Improvements to the OPTRAN approach", Appl. Opt., vol. 34, pp. 8396-8399, 1995
- [23] T. Meissner. and F.J. Wentz. "The Complex Dielectric Constant of Pure and Sea Water from Microwave Satellite Observations." *IEEE TGARS*, 42(9), pp. 1836 - 1849, 2004.
- [24] J.L Moncet, Isaacs, R.G. and Hegarty, J.D. "Application of the unified retrieval approach to real DMSP sensor data over ocean and land". Second Topical Symposium on Combined Optical-Microwave Earth and Atmosphere Sensing, 1995. Conference Proceedings. Pp-186-188, DOI: 10.1109/COMEAS.1995.472370, 1995
- [25] S. Padmanabhan; Reising, S.C.; Asher, W.E.; Rose, L.A.; and Gaiser, P.W., "Effects of foam on ocean surface microwave emission inferred from radiometric observations of reproducible breaking waves", IEEE Transactions on Geoscience and Remote Sensing, Volume 44, Issue 3, March 2006 Page(s):569 – 583. Digital Object Identifier 10.1109/TGRS.2006.870234
- [26] S. Padmanabhan; Reising, S.C.; Asher, W.E., "Azimuthal Dependence of the Microwave Emission from Foam Generated by Breaking Waves at 18.7 and 37 GHz", IEEE MicroRad, 2006. Feb. 28, 2006 Page(s):131 – 136. DOI 10.1109/MICRAD.2006.1677076
- [27] C. Prigent and P. Abba, "Sea surface equivalent brightness temperature at millimeter wavelength", *Annales Geophysicae*, 8, 627-634, 1990.
- [28] C.D. Rodgers, "Retrieval of Atmospheric Temperature and Composition From Remote Measurements of Thermal Radiation", *Reviews of Geophysics and Space Physics*, vol. 14, no 4, pp. 609-624, 1976
- [29] L.A. Rose, W.E. Asher, S.C. Reising, P.W. Gaiser, K.M. St Germain, D.J. Dowgiallo, K.A. Horgan, G. Farquharson and E.J. Knapp, "Radiometric Measurements of the Microwave Emissivity of Foam", IEEE Trans. Geosc. and Remote Sensing, 40,12, 2619-2625, 2002
- [30] B. Ruston and S. Boukabara. "An overview of current surface assimilation in NWP centers", Talk at the 1<sup>st</sup> Workshop on Remote Sensing and Modeling of Surface Properties, Paris, France, June 2006. <http://cimss.ssec.wisc.edu/itwg/groups/rtwg/meetings/sfcem/>
- [31] A. Stogryn. "Electromagnetic scattering from rough, finitely conducting surface". *Radio Sciences 2 (New Series)*, 4, 415–428, 1967
- [32] F. Weng, Y. Han, P. Van Delst, Q. Liu, T. Kleespies, B. Yan and J. Le Marshall, "JCSDA Community Radiative Transfer Model (CRTM)", Proceedings of the 14<sup>th</sup> TOVS conference, Beijing, China, 2005
- [33] F.J. Wentz, "Model function for ocean microwave brightness temperatures, J. Geophys. Res., 88, 1892-1908, 1983
- [34] T.T. Wilheit, "A model for the microwave emissivity of the ocean's surface as a function of wind speed". IEEE Trans. Geosc. and Remote Sensing, 17, 244-149, 1979

**S-A. Boukabara** (SM'06) received his Engineer and Master of Science degrees in signal processing from the *National School of Civil Aviation (ENAC)*, Toulouse, France and from the *Institut National Polytechnique de Toulouse*, France, respectively, both in 1994. He obtained his Ph.D. in remote sensing from the *Denis Diderot University* in Paris, France in 1997.

He was then involved in the calibration/validation of the European Space Agency (ESA)'s ERS-2 microwave radiometer and has worked on the synergistic use of active and passive microwave measurements. He then joined AER Inc. in Cambridge, Massachusetts, as a staff scientist and worked on the design, implementation and validation of the NPOESS/CMIS physical retrieval algorithm, on the NASA SeaWinds/QuikSCAT wind vector rain flag and on the development of the atmospheric absorption model MonoRTM, dedicated to the microwave and laser applications. He recently joined NOAA/NESDIS in Camp Springs, Maryland, and is leading an effort to develop the capability of assimilating passive microwave measurements in all-weather conditions using a combination of variational technique algorithm and the Community Radiative Transfer Model (CRTM). His principal areas of interest include radiative transfer modeling including absorption and scattering of the surface and the atmosphere, spectroscopy, algorithm development using neural networks, assimilation-type techniques and statistical approaches.

Dr Boukabara is a member of the American Meteorological Society (AMS) and the American Geophysical Union (AGU).

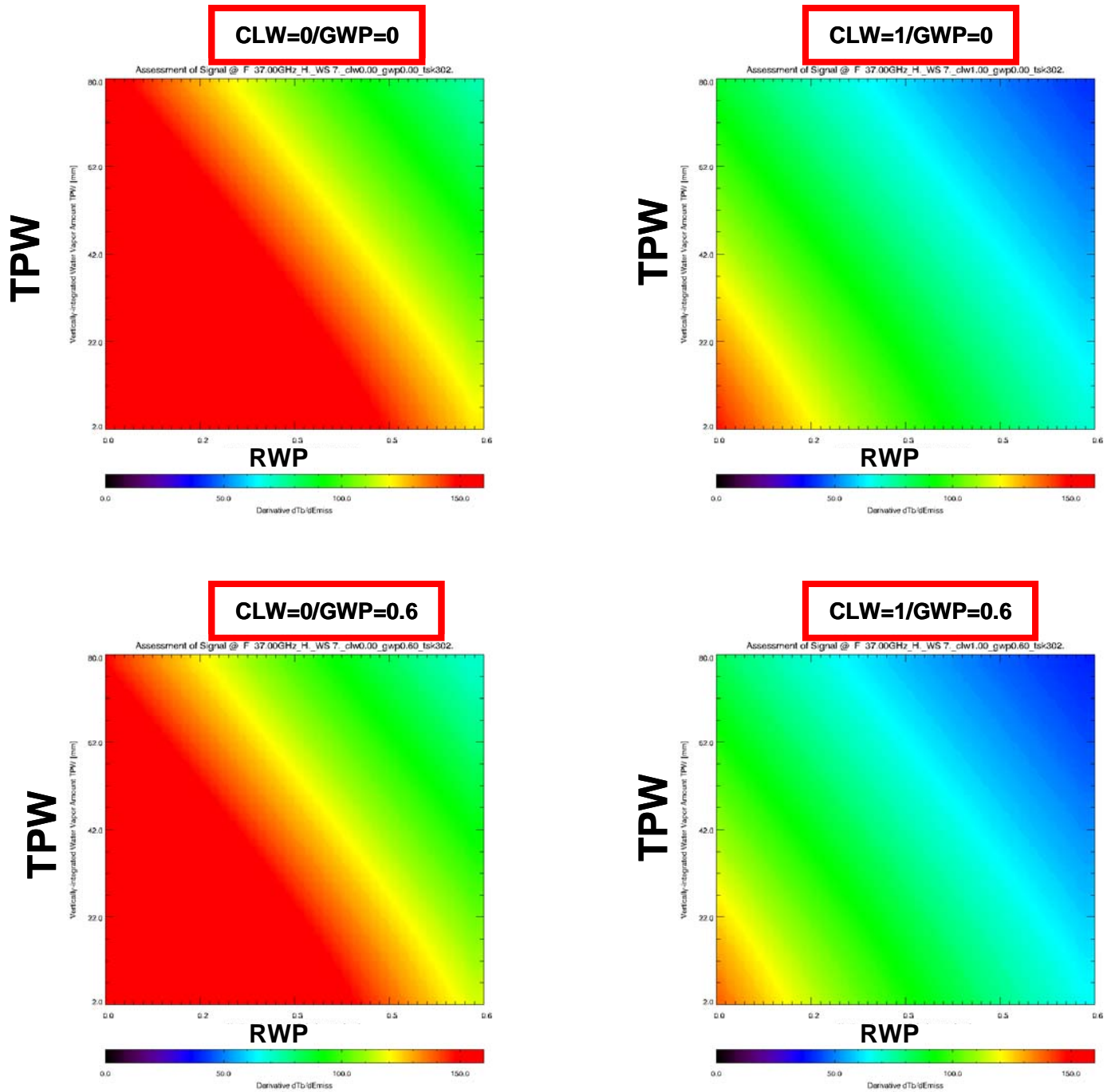


**Figure 1.** Sensitivity of the brightness temperature at 37 GHz (horizontal polarization) to emissivity as a function of both the total precipitable water (TPW) and the rain water path (RWP) for different combinations of integrated cloud liquid water (CLW) and graupel-size ice water path (GWP).

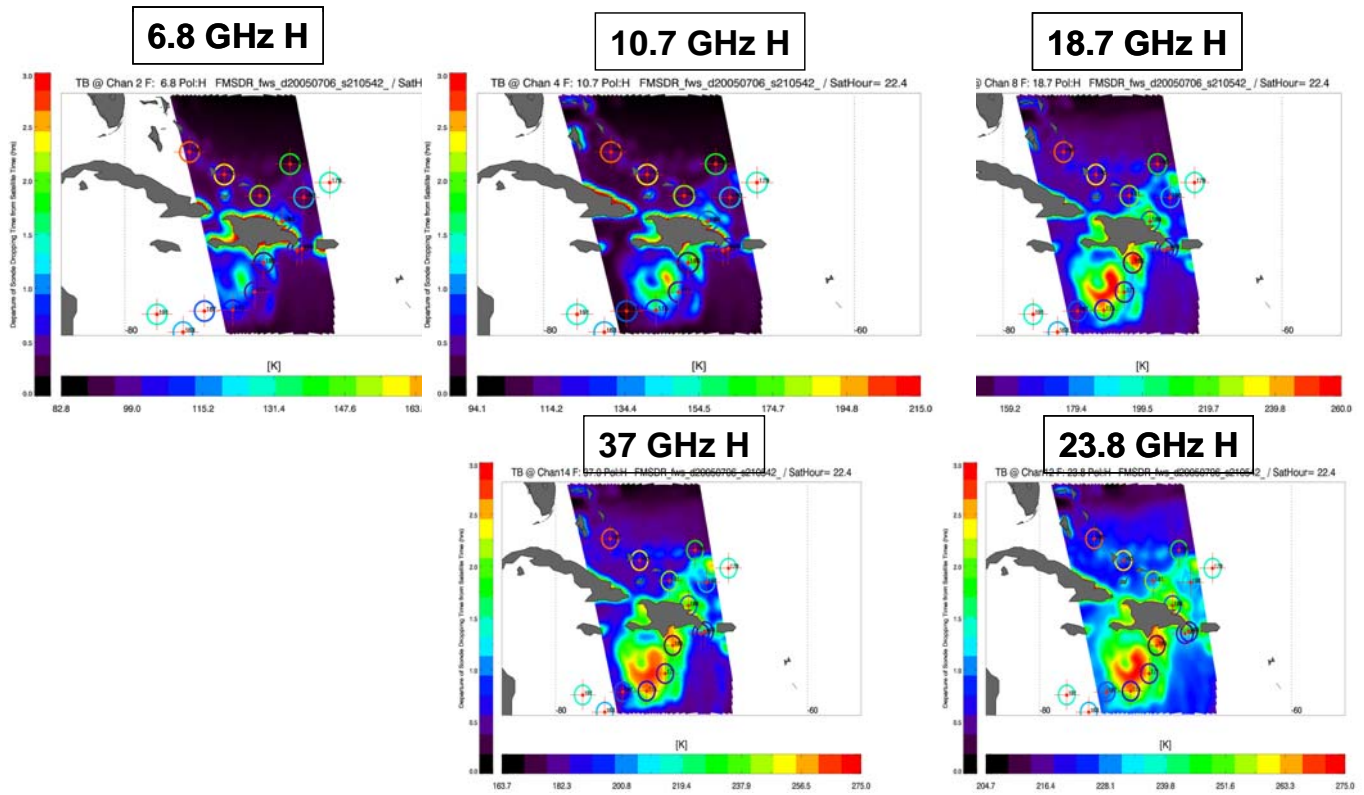


**Figure 2.** WINDSAT Brightness temperature responses during Hurricane Dennis in July 2005. Lower frequencies are less sensitive to atmospheric features. The locations of the dropwindsondes are overlaid. Note the narrower swath at 6.8 GHz channel.

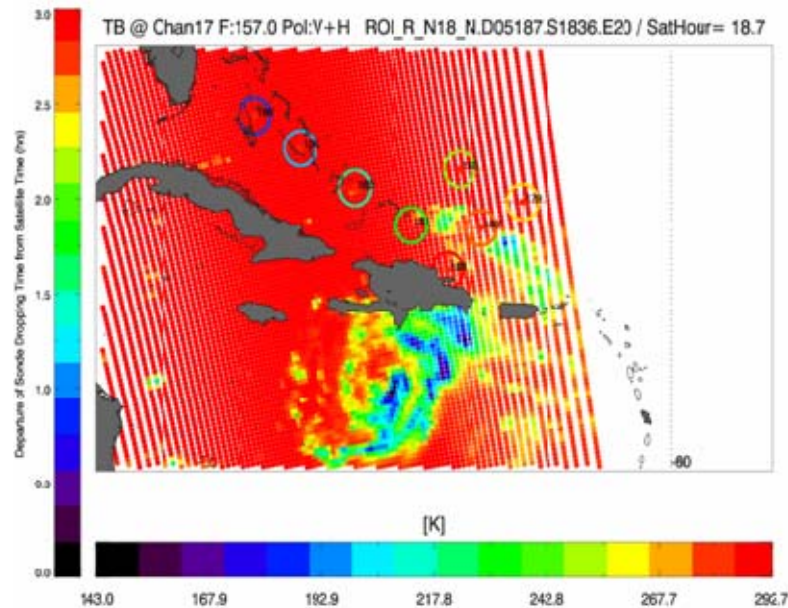


**Figure 3.** Signature of the NOAA-18/MHS 157 GHz channel of the same features depicted in Figure 2. Note that the measurements presented here occurred three (3) hours before the WINDSAT measurements. This channel is much more sensitive to precipitation and cloud than WINDSAT channels. Note that MHS swath is much wider with 90 scan positions within each scanline.

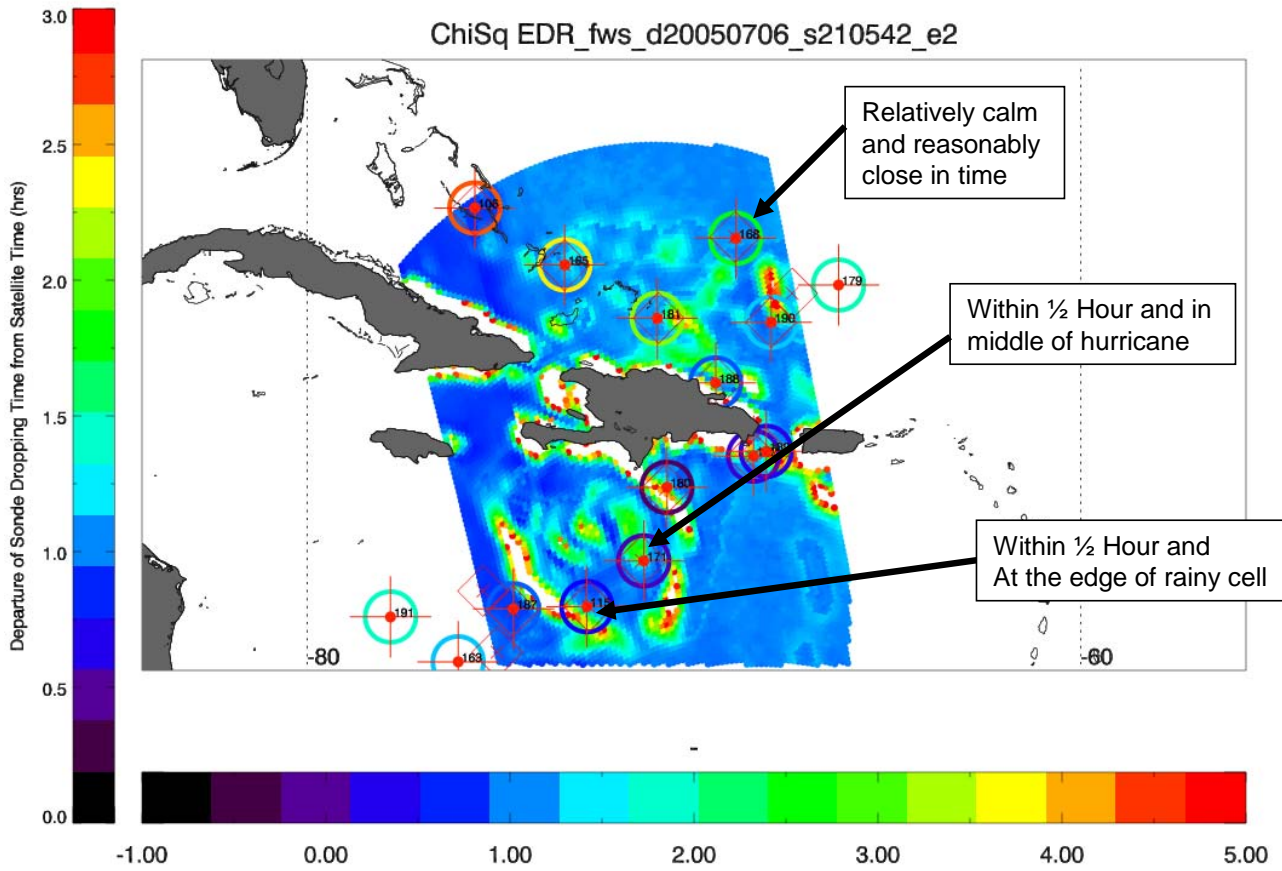


**Figure 4.** Horizontal display of the MIRS convergence metric and the overlaid locations of the GPS-dropwindsondes. A select few sondes were used to do a point-to-point comparison between emissivity spectra as computed from models (dropsonde-based wind used as input) and MIRS emissivity retrievals. These are highlighted in the plot above. Dropsondes labeled 168 and 171 were used later for the comparison in clear and rainy conditions respectively.

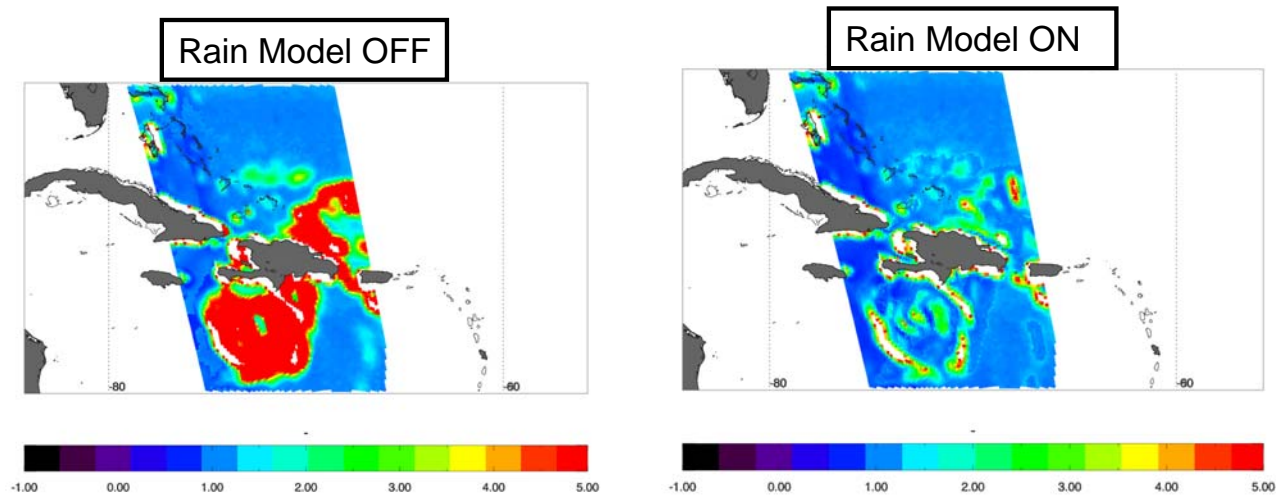


**Figure 5.** Horizontal display of the convergence metric when the multiple scattering is turned ON (right) and when it is turned OFF (left). Significant improvement is observed when the multiple scattering capability is used during the retrieval. Red color means non-convergence while blue means convergence. This does not mean that the retrieval vector is necessarily correct but at least the solution is radiometrically correct (by fitting the measurements). The 6.8 GHz channel is not present (and therefore not used) in the most left band of the swath which explains the subtle difference with the rest of the field.

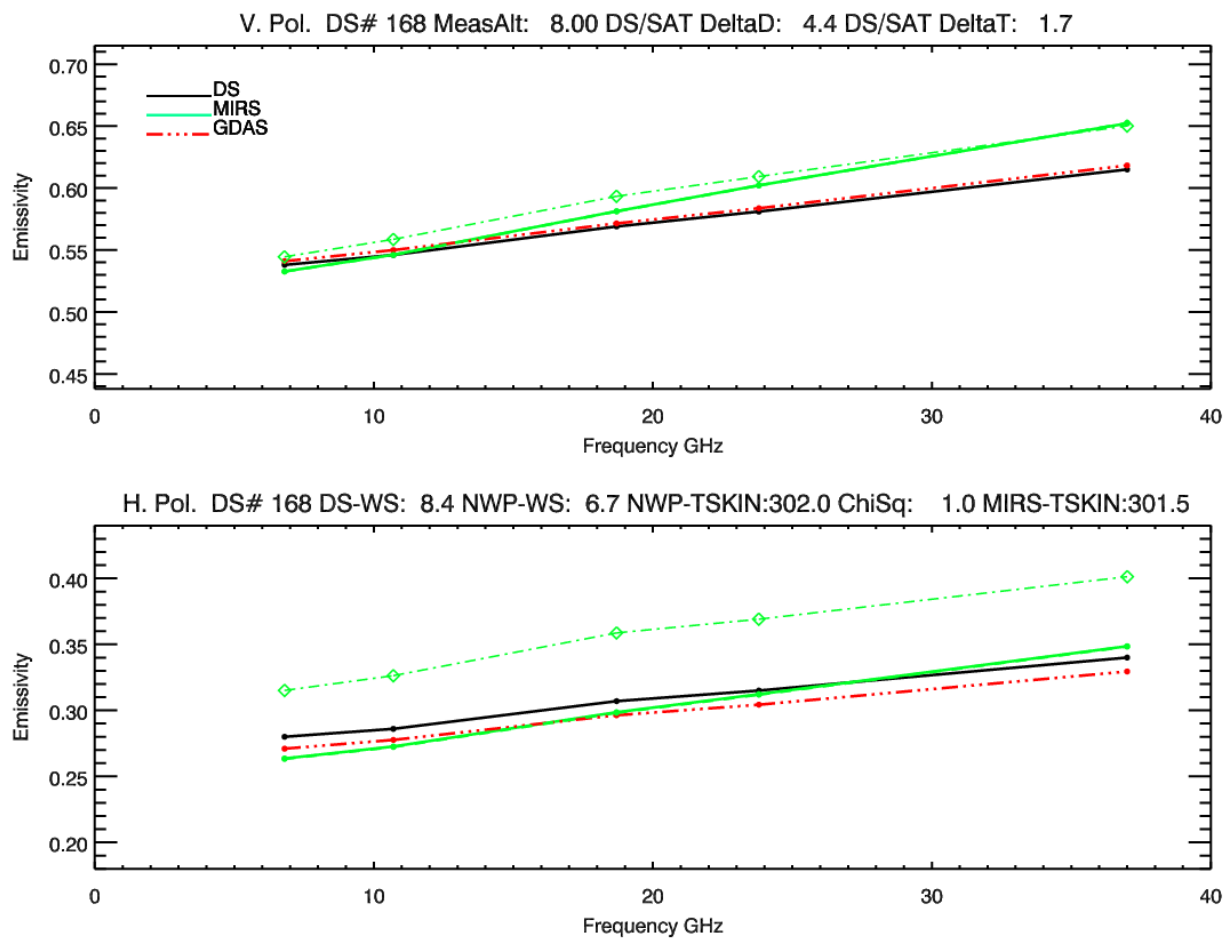


**Figure 6.** Case of a clear sky / calm sea. Spectra of emissivity (1) computed using FASTEM-3 emissivity model and GDAS winds as inputs (red, dotted-dashed), (2) using the GPS-dropwindsondes as inputs (black solid lines), and (3) retrieved using MIRS variational algorithm and WINDSAT brightness temperatures using two options (green solid: retrieval with multiple-scattering in the forward operator turned ON, green dashed when scattering OFF). In this plot (calm sea, clear sky) the two options give same retrievals. (4) The dotted-dashed green line is the background spectrum used as first guess in the MIRS. Vertical and Horizontal polarization channels are shown at the top and the bottom respectively. Along with the polarizations, the title also holds the dropsonde number (DS#) as well as the altitude (MeasAlt), the dropsonde/satellite time and distance differences (DeltaT and DeltaD), the skin temperatures (from GDAS and MIRS) and the wind closest to 10-meters height.

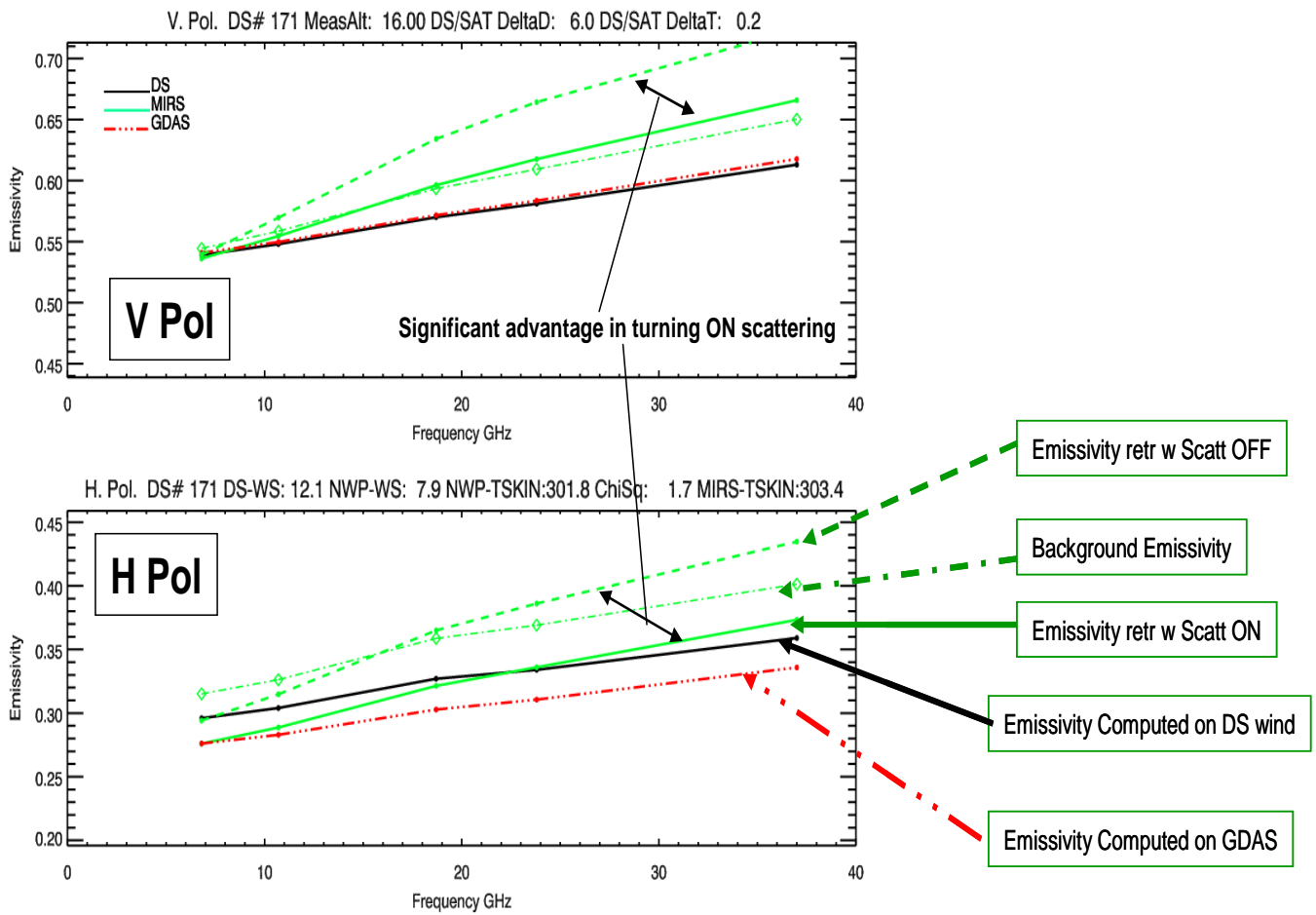


**Figure 7.** Comparison between GPS-based emissivities and MIRS-retrieved spectra for a single case in the middle of the hurricane (precipitating). V and H polarization channels are shown at the top and bottom panels respectively. In this case, there is a significant impact in using the multiple scattering ON (the spectrum is much different from when the scattering is turned OFF and absorption only is assumed).